pp 469–487. © Royal Aeronautical Society 2017
doi: 10.1017/aer.2017.11

Trajectory optimisation for a rocket-assisted hypersonic boost-glide vehicle

S.T.I. Rizvi
rizvi.aeng@gmail.com

H. Linshu and X. Dajun
School of Astronautics, Beihang University (BUAA)
Beijing
P.R. China

S.I.A. Shah
National University of Sciences and Technology
Islamabad
Pakistan

ABSTRACT

In this work, trajectory optimisation has been performed for a wing-body rocket assisted vehicle to compute the bestset of performance parameters including burn-out angle, angle-of-attack, bank-angle and throttle command that would result in optimal down-range and cross-range performance of the re-entry vehicle. An hp-adaptive Pseudospectral method has been used for the optimisation by combining the launch and rocket rocket-assisted re-entry stages. The purpose of the research is to compute optimal burn-out condition, angle-of-attack, bank-angle and optimal thrust segments that would maximise the down-range and cross-range performance of the hypersonic boost glide vehicle, under constrained heat rate environments. The variation of down-range/cross-range performance of rocket rocket-assisted hypersonic boost glide vehicle with bounds on diminishing heat rate has also been computed.

Keywords: trajectory optimisation; hypersonic boost-glide; waverider; wing-body configuration; pseudospectral method; optimal control

Received 21 May 2015; revised 1 September 2015; accepted 7 September 2015.

NOMENCLATURE

C	proportionality constant, $kg^{0.5}m^{1.5}/s^{3}$
C_D	coefficient of drag
C_L	coefficient of Lift
D	drag force, N
g	acceleration due to gravity, m/s^2
g_0	acceleration due to gravity at sea-level, m/s^2
Isp	specific impulse, s
L	lift force, N
L/D	lift-to-drag ratio
m	mass, kg
n_z	normal acceleration, g
Q	total heat load, J/m^2
$\dot{Q}$, Q'	heat transfer rate, W/m^2
q	dynamic pressure, Pa
Re	radius of earth, 6378×10^3 m
R	total range, m
S	reference area, m^2
t	time, s
V	velocity, m/s
α	angle-of-attack
β	inverse of density scale height, m
γ	flight path angle, deg or rad
Ψ	heading angle, deg or rad
Θ	longitude, deg or rad
Φ	latitude, deg or rad
ρ	density, kg/m^3
ρ_0	sea-level density, kg/m^3
μ	gravitational parameter, m^3/s^2
σ	bank angle
η	throttle ratio

1.0 INTRODUCTION

Waverider configuration has become extremely popular because of DARPA's X-41, Common Aero Vehicle (CAV) program and the Boeing X-51, scramjet jet-propelled experimental Hypersonic Cruise Vehicle (HCV). The waverider configuration has immense aerodynamic advantage because of the highest possible trim lift-to-drag ratio of greater than 3.0 in the hypersonic regime[1]. This high aerodynamic performance is not without any limitation. The waverider vehicle has a nose leading-edge radius of the order of 3-6 mm[2] and, therefore, experiences very high heating rates during the re-entry phase. Alternatively, the larger nose radius of the wing-body design has a better volumetric efficiency and also allows the use of conventional nose-mounted terminal sensors such as the millimetre wave radar. Common examples of wing-body vehicles are Shuttle-Orbiter and X-37B vehicles, with a trim lift-to-drag ratio of greater than 2.0[2,3]. The wing-body shapes face maximum heat-rate on the fin leading edges. With recent advancements in material technology (such as carbon-silicon

https://doi.org/10.1017/aer.2017.11 Published online by Cambridge University Press

carbide), and the availability of advanced materials capable of bearing temperatures up to 2,900 K[4], the utility of small wing-body design vehicles for medium and intermediate range applications cannot be ignored.

Re-entry studies performed in the past on wing-body configurations are mainly focused on Orbital Space Planes, Crew Return Vehicles and Manoeuvrable Re-entry Research Vehicles (MaRRV)[5-9]. Clarke[10] carried out trajectory optimisation of the re-entry trajectory of a CAV using the Legendre Pseudospectral Method. Jorris[11] carried out trajectory optimisation of a CAV using waypoint and no-fly zone as a constraint. Li[12,13] carried out trajectory optimisation of a Hypersonic Boost-Glide (HBG) waverider CAV configuration by modelling the boost phase. He computed the foot print of the CAV boosted from a Minuteman III boost vehicle to a speed of approximately 6.5 km/s and a burn-out angle of nearly 0° under a constrained heat rate environment. In almost all similar studies, re-entry speed greater than 6 km/s and re-entry angles less than 3° have been considered for intercontinental range. Rizvi et al[14] computed the optimal burn-out angles and subsequent optimal trajectories for the HBG waverider, with heat rate and integrated heat load constraint. The analysis showed that integrated heat load can be reduced by as much as 50%, with less than 10% range penalty, by optimising the burn-out angle and angle-of-attack. Another study by Rizvi et al[15] was carried out to compute the optimal burn-out angle and optimal re-entry trajectory for different shapes of HBG vehicles, using angle-of-attack and bank angle control for medium range application.

In the current work, the hp-adaptive pseudospectral method has been used to optimise the burn-out angle and subsequent re-entry trajectory of a rocket rocket-assisted, wing-body hypersonic vehicle using angle-of-attack, bank angle and throttle control. The dependence of burn-out conditions on the vehicle performance is demonstrated for an HBG waverider, wing-body type HBG vehicle and a rocket rocket-assisted wing-body vehicle under the constrained heat-rate environment. The multiphase optimisation problem for three types of vehicles i.e. waverider, wing-body glide and wing-body rocket assisted vehicle, has been considered with the heat rate limit of 4 MW/m^2, which is computed at the nose of a waverider and at the fin-tip location of a wing-body missile. The effect on performance of the rocket assisted boost vehicle with the lowering of the heat rate limit has been computed. The system performance has been evaluated for the heat rate limits of 2 MW/m^2, 3 MW/m^2 and 4 MW/m^2, which correspond to stagnation point temperatures of 2,500K, 2,775K and 2,975K, respectively, under the radiation equilibrium condition.

As a result of this research, the optimal burn-out conditions for the launch vehicle, and subsequent optimal trajectory and control deflections of the rocket rocket-assisted wing-body configurations, have been successfully computed, which should result in maximum down-range and cross-range performance of the vehicle systems, under the constrained heat rate environment. Comparative performance analysis with wing-body and waverider configuration has been done. This multi-phase, non-linear optimal control problem has been solved using hp-adaptive pseudospectral method.

2.0 PHYSICAL MODEL

2.1 Launch and re-entry vehicle data

The vehicle data of the launch vehicle and the two types of re-entry vehicles under consideration, along with applicable physical constants have been presented in Tables 1 and 2, respectively. The nose radius is denoted by R_N, whereas the fin radius and fin sweep angle are denoted by R_F and Λ_F. The physical properties of the wing-body glide vehicle are considered

https://doi.org/10.1017/aer.2017.11 Published online by Cambridge University Press

Table 1
Launch vehicle data

Quantity	Numerical Values
Propulsion	Solid
Body Diameter, m	1.4
Booster 1	
Mass, [kg]	16,300
Propellant Mass, [kg]	13,700
Empty Mass, [kg]	2,600
Thrust, [N]	398,000
Isp, [s]	237
Booster 2	
Mass, [kg]	3,800
Propellant Mass, [kg]	3,250
Empty Mass, [kg]	650
Thrust, [N]	97,000
Isp, [s]	250

Table 2
Re-entry vehicle data and physical constants

Configuration	Quantity	Numerical Values
Waverider	*Mass, [kg]	900
	W/S, [kg/m^2]	400
	R_N, [m]	0.006
	C_{WR},[kg$^{0.5}$m$^{1.5}$/s^3]	1.1813×10^{-3}
Rocket Assisted Wing-body	Mass, [kg]	1,300
	W/S, [kg/m^2]	400
	Thrust, [N]	3,820
	Empty Mass, [kg]	910
	Isp,[s]	295
	R_N, [m]	0.075
	Λ_F, degrees	75
	C_{FIN},[kg$^{0.5}$m$^{1.5}$/s^3]	9.12×10^{-4}

*Mass of waverider and wing-body boost-glide configuration

to be the same as that of the rocket assisted wing-body vehicle, except that the mass of the wing-body glide vehicle is 900 kg as opposed to 1,300 kg for the rocket assisted vehicle. The planform-loading for lifting-body, wing-body as well as waverider configuration is assumed to be 400 kg/m^2, which is consistent with that of fighter aircraft as well as MaRRV data considered by Zimmerman and Calise[5], Gogu et al[6] and Darby and Rao[16].

The launch vehicle is a two stage boost vehicle, with a launch mass of 21,550 kg and payload mass of 1,300 kg. With 900 kg of payload instead, the launch mass reduces to 20,650 kg.

https://doi.org/10.1017/aer.2017.11 Published online by Cambridge University Press

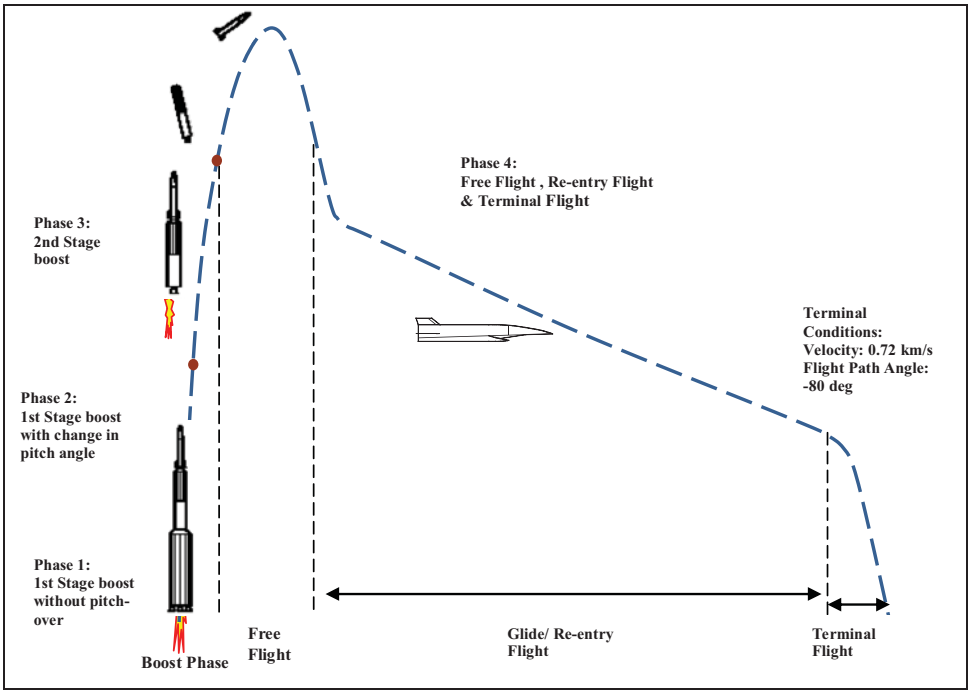

Figure 1. (Colour online) Schematics for boost-glide missile trajectory design problem.

2.2 Definition of phases

The optimisation problem has been divided into four phases to handle discontinuities in control mode and mass loss at the end of each boost stage. These phases of flight are described below and depicted in Fig. 1.

1. **The first 5 seconds of first stage boost phase, during which pitch manoeuvre does not take place.** In this phase, the vehicle gains sufficient speed in the first 5 seconds, after which the stabilisers become effective and provide sufficient damping moment for a controlled pitch manoeuvre[17].
2. **The time duration after t = 5s till the burn-out of the first stage rocket motor**. It is during this phase that the launch vehicle pitches down using angle-of-attack control.
3. **The second stage boost phase**. In this phase, the flight path angle changes to meet the burn-out conditions.
4. **The free flight and the re-entry stage**. In this phase, the vehicle is steered to optimal down-range or cross-range distance with the help of angle-of-attack, bank angle and throttle control.

The states at the end of the third phase, which include the burn-out angle, burn-out altitude and the burn-out speed are treated as free parameters and, therefore, can be optimised. The fourth phase includes the free flight phase as well as the re-entry phase. This approach, which encompasses modelling and simulation of the launch phase, gives the best burn-out angle and

https://doi.org/10.1017/aer.2017.11 Published online by Cambridge University Press

the burn-out altitude required for the maximum down-range and cross-range trajectories under constrained heat rate limits. The empty weight mass lost at the end of each stage is described in a separate linkage file which connects all the states from one phase to another.

2.3 Earth and the atmosphere

The earth has been assumed to be a perfect, non-rotating sphere. The acceleration due to gravity is given by Newton's inverse square law as given in Equation (1). The atmosphere is modelled using 1976 ICAO atmospheric model.

$$g = \frac{\mu}{r^2}, \quad \ldots (1)$$

where μ is the gravitational constant and is equal to $3.986 \times 10^{14}\ \mathrm{m}^3/\mathrm{s}^2$.

2.4 Aerodynamic model

An integrated wave-rider has a lift-to-drag ratio close to four at Mach 4.0[1]. The aerodynamic model for the waverider configuration was obtained using the experimental data of Crockrell[1]. Equations (2) and (3) represent the aerodynamic model of a waverider.

$$C_L = -0.03 + 0.75\alpha, \quad \ldots (2)$$

$$C_D = 0.012 - 0.01\alpha + 0.6\alpha^2 \quad \ldots (3)$$

The following set of equations represents the aerodynamic model of a wing-body vehicle obtained from shuttle trim aerodynamic data, presented by Surber and Oslen[3].

$$C_L = -0.034 + 0.93\alpha, \quad \ldots (4)$$

$$C_D = 0.037 - 0.01\alpha + 0.736\alpha^2 + 0.937\alpha^3 \quad \ldots (5)$$

C_L and C_D are assumed to be functions of the angle-of-attack (α) only. This is true in the hypersonic region in which the aerodynamic coefficients do not vary with Mach number[18]. The effect of Reynold's number on lift and drag coefficients has been neglected. The variation of lift-to-drag ratio for waverider and wing-body vehicles in the hypersonic regime is represented in Fig. 2.

2.5 Equations of motion

The following set of equations of motion is used for the 3 degree of freedom (DOF) point mass model. The equations have been extensively used in the study of re-entry vehicles and their guidance systems[5,6,16].

$$\frac{dr}{dt} = V \sin\gamma, \quad \ldots (6)$$

$$\frac{d\Theta}{dt} = \frac{V \cos\gamma \sin\psi}{r \cos\phi}, \quad \ldots (7)$$

$$\frac{d\Phi}{dt} = \frac{V \cos\gamma \cos\psi}{r}, \quad \ldots (8)$$

https://doi.org/10.1017/aer.2017.11 Published online by Cambridge University Press

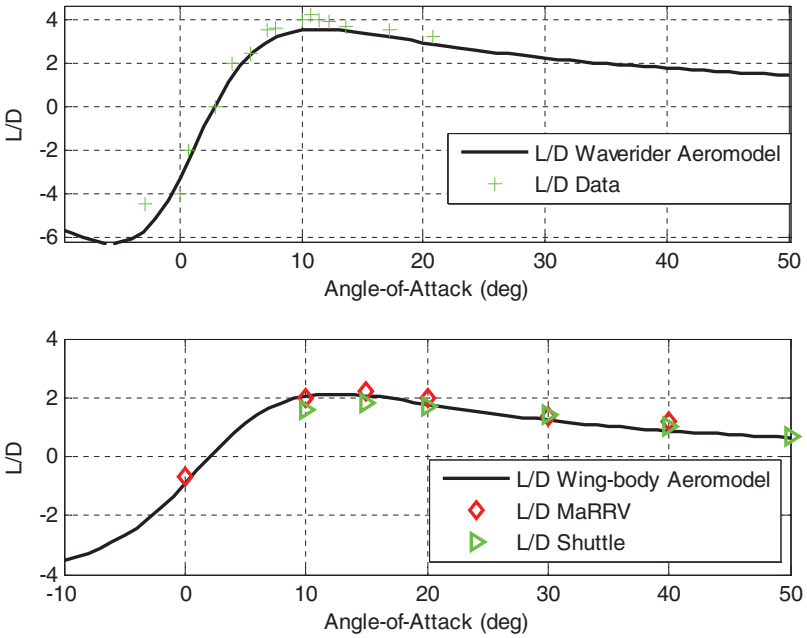

Figure 2. (Colour online) Lift to drag ratio vs. angle-of-attack (a) waverider (b) wing-body vehicle.

$$\frac{dV}{dt} = \frac{T}{m}\cos\alpha - \frac{D}{m} - g\sin\gamma, \qquad \ldots(9)$$

$$\frac{d\gamma}{dt} = \frac{1}{V}\left[\left(\frac{T}{m}\sin\alpha + \frac{L}{m}\right)\cos\sigma - \left(g - \frac{V^2}{r}\right)\cos\gamma\right], \qquad \ldots(10)$$

$$\frac{d\psi}{dt} = \frac{1}{V}\left[\left(\frac{T}{m}\sin\alpha + \frac{L}{m}\right)\frac{\sin\sigma}{\cos\gamma} + \frac{V^2\cos\gamma\sin\psi\tan\varphi}{r}\right], \qquad \ldots(11)$$

$$\frac{dm}{dt} = \frac{-T}{I_{sp}.g_0}, \qquad \ldots(12)$$

where r is the radial distance from the centre of the earth to the re-entry vehicle, Θ and φ are the longitude and latitude, respectively, V is the total velocity of the vehicle, γ and ψ are the flight path angle and the azimuth angles, respectively, whereas m is the mass. The terms L and D are defined as $L = 0.5C_L\rho V^2 S$ and $D = 0.5C_D\rho V^2 S$. Thrust has been assumed to be zero for the boost-glide vehicle, whereas for the rocket assisted wing-body vehicle, it is a function of throttle ratio (η).

2.6 Stagnation point heat rate

The equation for convective heat transfer rate is given by Scott et al[19]:

$$\dot{Q} = C_{WR}\rho^{0.5}V^{3.05} \qquad \ldots(13)$$

https://doi.org/10.1017/aer.2017.11 Published online by Cambridge University Press

The convective heat transfer at the fin tip or the wing leading edge is calculated using Equation (14) below, which is valid for swept cylinder with cylinder radius R_F inclined at a sweep angle, Λ_F to the flow[20]. It has been assumed in Equation (14) that the enthalpy at the wall is very small as compared to that of infinite value, which is only true for the no-slip condition. For the slip condition, less heat is generated because of less skin friction as compared to the no-slip case.

$$\dot{Q}_F = C_{FIN}\sqrt{\rho}V^3(1 - 0.18\sin^2\Lambda)\cos\Lambda \quad \ldots(14)$$

The total heat load at the stagnation point is calculated using the relationship:

$$Q = \int_{t_0}^{t_f} \dot{Q}dt, \quad \ldots(15)$$

where t_0 and t_f are the initial and final time in the free-flight and re-entry phase.

2.7 Normal acceleration

For a winged body, the normal acceleration is of greater importance as compared to the total deceleration load. The normal acceleration is computed using the relation given in Equation (16).

$$n_z = \frac{L\cos\alpha + D\sin\alpha}{mg} \quad \ldots(16)$$

2.8 Controls

The waverider vehicle has controls for both angle-of-attack and bank-angle. The vehicle is assumed to have angle-of-attack trim capability from a $-10°$ to $50°$ angle-of-attack and a bank angle control of $\pm 90°$. The angle-of-attack control modulates the lift as well as the heat rate. The bank angle results in a lateral force which causes the sideward motion of the spacecraft.

The rocket-assisted wing-body vehicle has an additional throttle control. Thrust is modulated by changing the throttle ratio (η). The variation of thrust with throttle control is given by the relation: $T = \eta T_{\max}$, where η varies from 0 to 1.

The launch-vehicle also has an angle-of-attack control. The angle-of-attack range during the launch phase has been set between $\pm 20°$. The controls can be expressed as:

$$u_1 = \alpha;\ u_2 = \delta;\ u_3 = \eta;\ u_2 = \delta;\ u_3 = \eta \quad \ldots(17)$$

3.0 BOUNDARY CONDITIONS AND CONSTRAINTS

The initial conditions are the conditions of the missile at the launch pad, which are:

$$r(i) = 6378 \times 10^3\ \text{km};\ \Theta(i) = 0;\ \varphi(i) = 0.0;\ V(i) = 0.0\ \text{m/s};\ \gamma(i) = 90\ \text{deg};\ \psi = 90\ \text{deg};\ m = m0 \quad \ldots(18)$$

The terminal boundary conditions correspond to penetration requirements of a conventional warhead. It is desirable that the warhead may be able to strike the target at a maximum possible

https://doi.org/10.1017/aer.2017.11 Published online by Cambridge University Press

velocity and at a high impact angle close to 90°. Too high an impact speed improves the performance of the warhead alone, but raises the maximum dynamic pressure limit of the re-entry body. This implies a higher structural limit and higher empty weight. For the current study the maximum terminal speed is considered to be 720 m/s at an impact angle of 80°. The requirement has been modelled as a terminal constraint.

$$r(f) = 6378\,\text{km};\ V(f) = 720\,m/s;\ \gamma(f) = -80\,\text{deg} \qquad \ldots(19)$$

The path constraint imposed on the trajectory is the heat rate constraint which is directly linked to the surface temperature in radiative equilibrium with the surroundings. The carbon-carbon composite material can retain its properties till a temperature of 2,900°K[4]. This temperature corresponds to the heat rate limit of approximately 4.0 MW/m^2. Performance variation at a reduced heat rate bound of 3 MW/m^2 and 2.0 MW/m^2 has also been studied here. Mathematically the constraint can be expressed as in Equation (20) below. The surface temperature can be computed using Equation (21). This equation is valid on the assumption that convective heat transfer is balanced by radiative heat transfer away from the body.

$$\dot{Q} \leq 4.0\,\text{MW/m}^2,\ 3.0\,\text{MW/m}^2,\ 2.0\,\text{MW/m}^2 \qquad \ldots(20)$$

$$\dot{Q} = \sigma\varepsilon_{th}(T_g^4 - T_w{}^4), \qquad \ldots(21)$$

where σ is the Stefan-Boltzmann constant, which is equal to 5.67×10^{-8} $\text{W/(m}^2\text{.K}^4\text{)}$, and ε_{th} is the surface emissivity which is generally close to 0.9.

4.0 METHODOLOGY

The optimal control, launch and re-entry problem, is solved to find the optimal state vector and the corresponding control deflections that minimise the cost function, subject to the dynamic constraints of Equations (6)-(12), the initial and terminal flight path constraints of Equations (18) and (19), respectively, and the path constraints of Equation (20).

The non-linearity in this optimal control problem is solved using an hp-adaptive method implemented in open source Gauss Pseudospectral Optimization Software (GPOPS) version 4.0. In the hp-adaptive technique, the number of nodes and the number of collocation points are determined at the end of the iteration. The mesh is further refined in areas where the constraints are not met, even by the increasing of the degree of the Lagrange Polynomial. The mesh refinement continues till a solution is obtained which satisfies error tolerance[21]. The details of the hp-adaptive algorithm are given in Ref. 22. For the current research, the maximum number of mesh iterations was set to 12, with nodes varying from 4 to 10. The error tolerance was set to 1e-3. The Non-linear Programming (NLP) derivatives were computed using a finite difference scheme.

5.0 RESULTS

The numerical optimisation results for this non-linear, multi-stage optimisation problem with the objective of maximising the down-range and the cross-range of waverider, wing-body boost-glide vehicles and rocket assisted wing-body vehicles, are tabulated in Table 3. The results show that the waverider vehicle has the maximum range performance, followed by the rocket assisted wing-body and, subsequently, the wing-body glide vehicle. The waverider

https://doi.org/10.1017/aer.2017.11 Published online by Cambridge University Press

Table 3
Numerical results for lifting vehicle performance with heat rate constraints

Configuration	$\dot{Q}_{max}$ [MW/m^2]	Down-Range [km]	Cross-Range [km]	γ_3(f) [deg]	V_3(f) [km/hr]	h_3(f) [km]	Q [GJ/m^2]	n_{zmax} [g]	Time [min]
Waverider	4.01	**4,158**	0.00	4.72	4.18	66.8	2.2563	3.02	28.33
(mass 900 kg)	4.01	*1932.5*	**2,072.0**	0.5	4.17	55.27	1.970	1.82	25.6
Wing-body	4.19	**3,105.3**	0.00	12.28	4.15	91.37	0.4598	6.64	20.3
(mass 900 kg)	2.9+	*1,515.3*	**944.3**	0.84	4.18	60.33	0.52	4.86	14.92
Rocket assisted	4.0	**3,780**	0	10.9	3.70	82.9	0.74	5.1	23.15
Wing-body	3.0	3,630	0	7.7	3.74	73.0	0.81	2.7	22.54
(mass	2.0	3,450	0	6.0	3.74	66.6	0.82	1.8	21.84
1300 kg)	4.0	1,700	**1,405**	1.34	3.76	59.7	0.67	4.7	17.7
	3.0	1,675	1,400	0.78	3.75	57.5	0.68	3.2	17.6
	2.0	1,645	1,370	0.5	3.73	52.8	0.68	1.7	17.5

*Max cross-range results; +optimal max heat rate

vehicle has the lowest burn-out angle of 4.72°. It loses speed gradually due to drag-force and maximum kinetic energy gets converted into range, with the entire flight within the atmosphere, as shown in Fig. 3.

For the wing-body configuration, which is a low performance vehicle as compared to a waverider, it is needed to maximise the total range by optimising the free flight range and the glide range. This is obviously possible at a certain burn-out angle such that: (a) the re-entry angle does not become sharp enough to violate the heat rate constraint, (b) the angle-of-attack after re-entry does not become too high to lose kinetic energy due to drag force. It is because of these reasons that the optimal burn-out angle for the wing-body glide vehicle is approximately 12.3° at a burn-out speed of 4.15 km/s, and for the heat rate constraint of 4 MW/m^2 computed at the fin.

For the rocket assisted boost vehicle, the launch vehicle is only able to accelerate to a speed of 3.7 km/s because of greater payload weight as compared to wing-body glide vehicle. The optimisation results show that for optimal down-range performance, the liquid rocket motor ignites immediately after the launch phase is over, thereby increasing the re-entry speed to 4.6 km/s as shown in Figs 4 and 5. This implies that the burn-out angle needs to be lowered such that the heat rate bound is not violated and the angle-of-attack remains in a range such that minimum energy is lost due to drag and heat. The optimisation algorithm in this case computes the optimal burn-out angle as 10.9° for the maximum down-range performance. Figure 4 shows the trajectory shapes on an altitude vs. velocity map with the heat rate constraint line. The figure shows that in none of the cases, the heat rate bound is violated. The heat profile is shown in Fig. 6(a) which shows that the waverider vehicle experiences higher integrated heat load. Integrated heat values are tabulated in Table 3, column 8. The integrated heat values computed at the waverider nose stagnation point are almost thrice as much as compared to those computed at the fin stagnation point of the rocket assisted wing-body configuration. The integrated heat values are lower for the wing-body vehicles as compared to the waverider configuration, primarily because optimal wing-body trajectories

https://doi.org/10.1017/aer.2017.11 Published online by Cambridge University Press

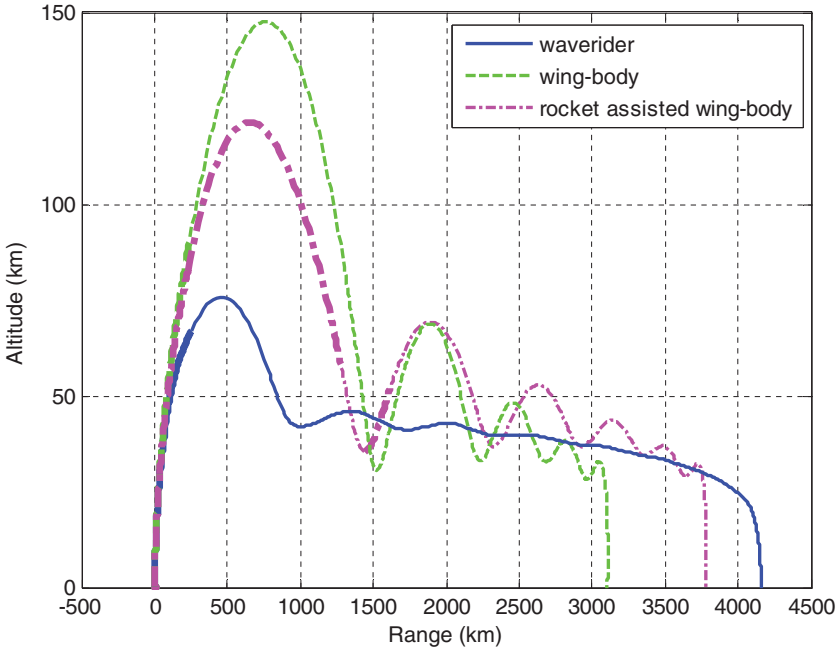

Figure 3. (Colour online) Altitude vs. range plot for different lifting vehicles and objective to maximise down-range at maximum heat rate constraint of 4 MW/m^2.

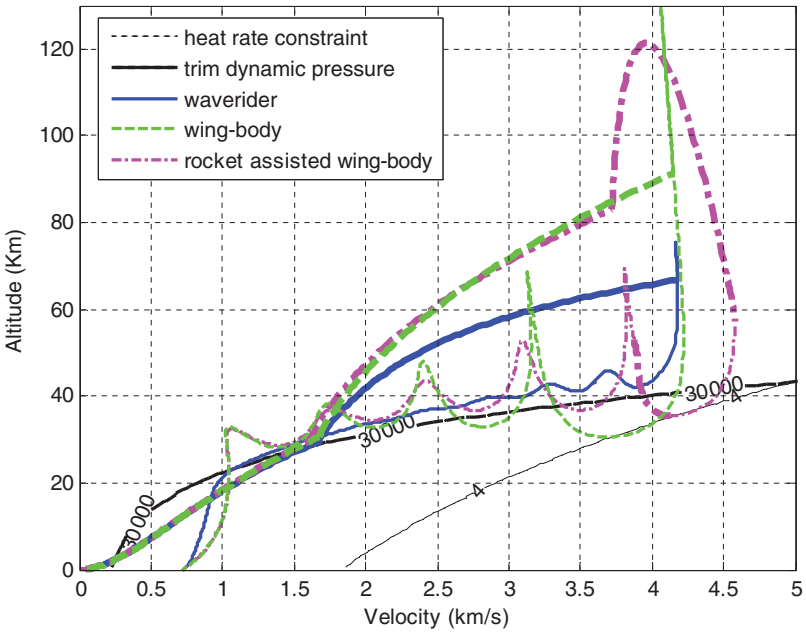

Figure 4. (Colour online) Optimal trajectory shapes for different lifting vehicles and objective to maximise down-range.

https://doi.org/10.1017/aer.2017.11 Published online by Cambridge University Press

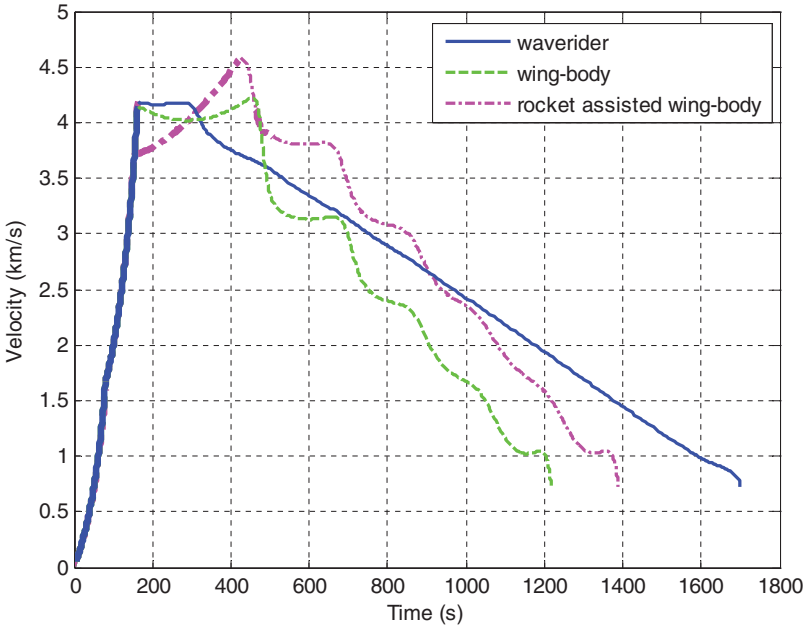

Figure 5. (Colour online) Velocity vs. time plot for different lifting vehicles and objective to maximise down-range at maximum heat rate constraint of 4 MW/m^2.

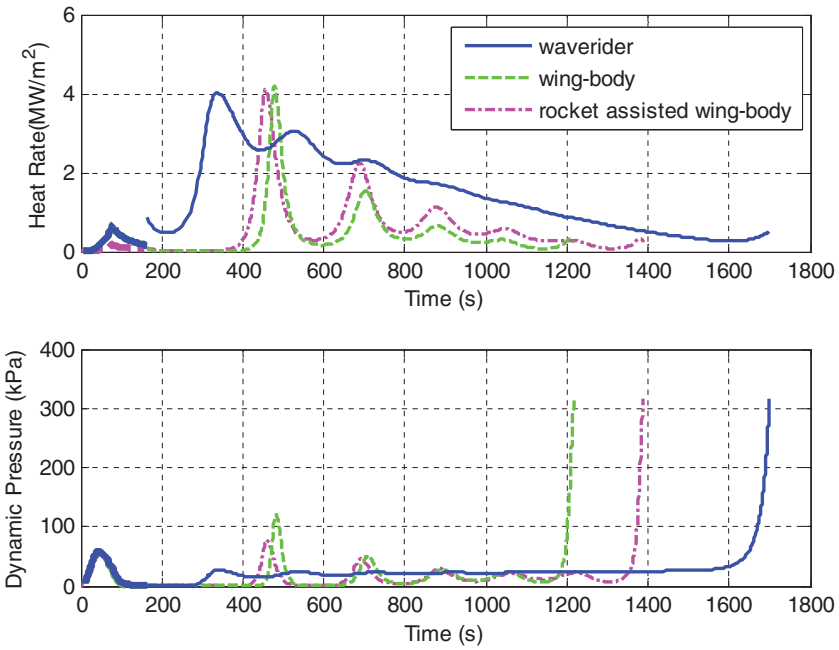

Figure 6. (Colour online) (a) Heat rate vs. time and (b) dynamic pressure variation with time lifting vehicles and objective to maximise down-range at maximum heat rate constraint of 4 MW/m^2.

https://doi.org/10.1017/aer.2017.11 Published online by Cambridge University Press

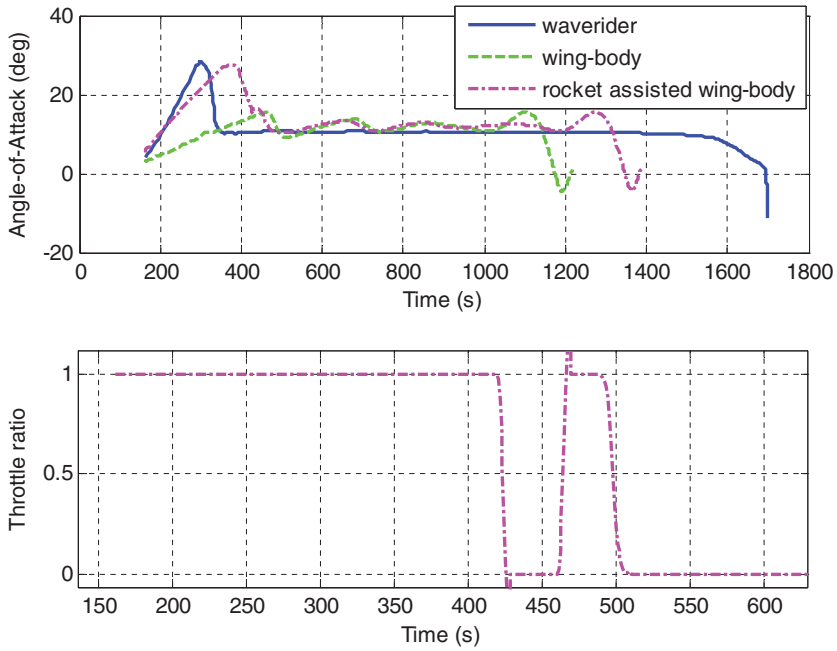

Figure 7. (Colour online) (a) Angle-of-attack and (b) throttle control variation with time; for different lifting vehicles and objective to maximise down-range at maximum heat-rate constraint of 4 MW/m^2.

have a phugoid type motion, and the vehicle spends more time in the high altitude region, resulting in lower heat rates with time, and therefore, lead to lower integrated heat values.

The angle-of-attack variation with time is shown in Fig. 7(a), which shows that for the waverider vehicle, the maximum angle-of-attack reaches almost 20° so as to arrest the descent rate after burn-out and to remain within the required heat rate bound. The vehicle flies a constant dynamic pressure trajectory, while maintaining 30,000 Pa as shown in Figs 5 and 6(b). The angle-of-attack corresponding to the optimal glide trajectory is 10°, which is the same as the angle-of-attack corresponding to the maximum lift-to-drag ratio for the waverider configuration according to the aerodynamic model depicted in Equations (2) and (3). For the wing-body vehicle, the maximum angle-of-attack attained is almost 18°, while for the rocket assisted wing-body vehicle, the maximum angle-of-attack goes to approximately 28° remaining within the heat rate bound at re-entry speed of approximately 4.6 km/s. During the mid-course phase, the angle-of-attack remains between 10° to 15°. This is the region in which lift-to-drag is maximum as shown in Fig. 2.

The throttle position as a function of time is shown in Fig. 7(b), which shows that the variable throttle liquid rocket engine ignites with full thrust immediately after the burn-out of the second stage solid propellant rocket motor. The throttle position comes to zero immediately after the re-entry. This is accompanied by an increase in angle-of-attack to execute an ideal pull up manoeuvre, followed by a skip trajectory. The throttle position goes to maximum again after the vehicle starts to gain altitude. The thrust phases of the solid rocket and the liquid rocket engine are shown in thick lines in all the figures. The two-stage thrust phase of the liquid propulsion engine can be observed in Figs 3-5.

https://doi.org/10.1017/aer.2017.11 Published online by Cambridge University Press

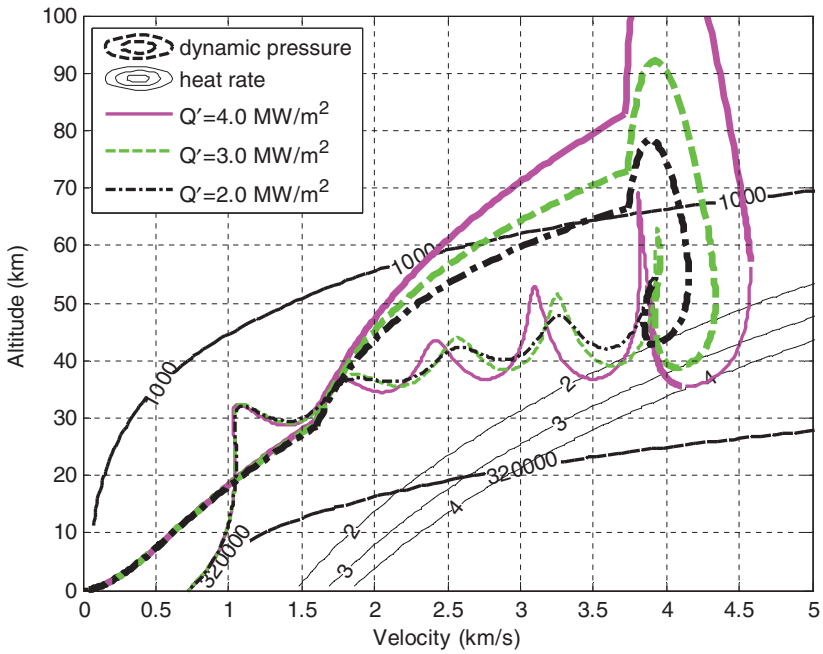

Figure 8. (Colour online) Optimal trajectory shapes for surface launch rocket assisted wing-body vehicle and objective to maximise down-range at different heat rate constraints.

These results show that the cross-range performance of the waverider exceeds that of the rocket assisted wing-body vehicle by about 32% under the constrained heat rate environment as shown in Table 3.

For cases where the objective is to maximise the cross-range performance, with unconstrained down-range, the optimal burn-out condition is almost zero-degree burn-out angle. This is because it has been ensured through the proposed optimisation that the system is within the atmosphere with enough dynamic pressure to sustain the turn rate and utilise its kinetic energy to attain optimal cross-range performance.

The detailed trajectory optimisation results for the rocket assisted wing-body vehicle with variation in heat rate constraint, and with the objective to maximise the down-range performance, are shown in Figs 8-10. The results show that as the heat rate constraint is lowered , the optimal burn-out angle reduces. The range values in Table 3 show that when the maximum allowable heat rate is reduced from 4 MW/m^2 to 2 MW/m^2, the down-range is reduced by only 8.7%.

The altitude variation with time is shown in Fig. 9. The plot shows that in the optimal trajectories, which are constrained by lower heat rate bounds, energy is quickly depleted due to drag force because of burn-out at lower altitudes and a lower flight path angle, resulting in a lower range. The angle-of-attack and throttle control as a function of time are shown in Fig. 10(a) and (b), respectively. The maximum angle-of-attack remains less than 30° in all cases. The throttle control adjusts to optimise down-range, while avoiding the heat rate boundary.

The cross-range optimisation trajectories and corresponding control deflections for the rocket boosted wing-body hypersonic vehicle with constrained heat rates are shown in

https://doi.org/10.1017/aer.2017.11 Published online by Cambridge University Press

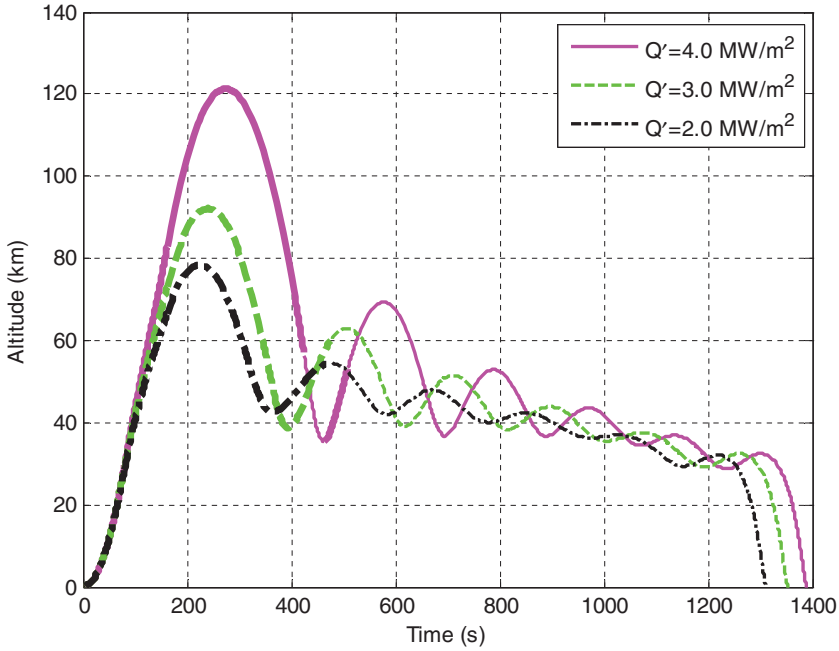

Figure 9. (Colour online) Altitude vs. time for surface launch wing-body vehicle with boost phase, and objective to maximise down-range at different heat rate constraints.

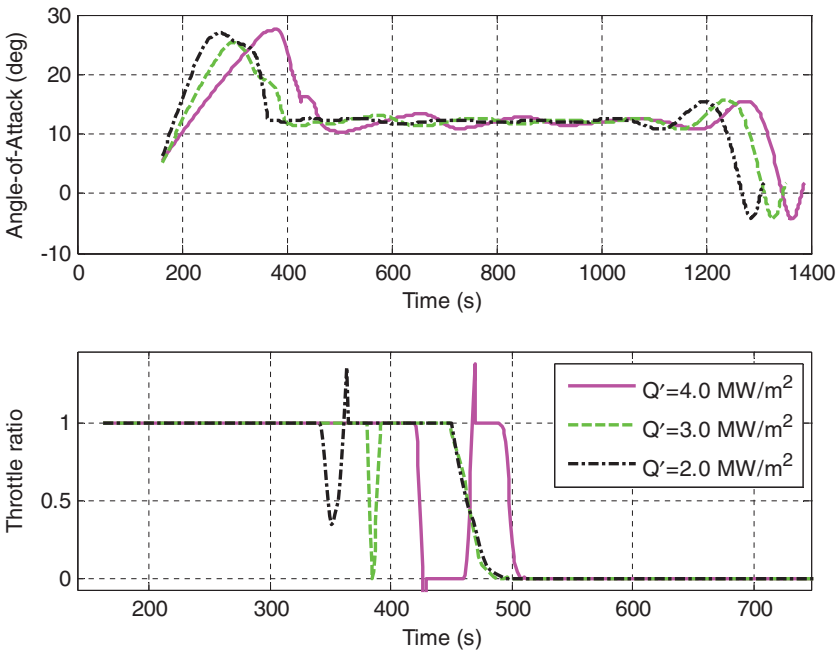

Figure 10. (Colour online) (a) Angle-of-attack vs. time and (b) throttle ratio vs. time for surface launch rocket assisted wing-body vehicle and different heat rate constraints.

https://doi.org/10.1017/aer.2017.11 Published online by Cambridge University Press

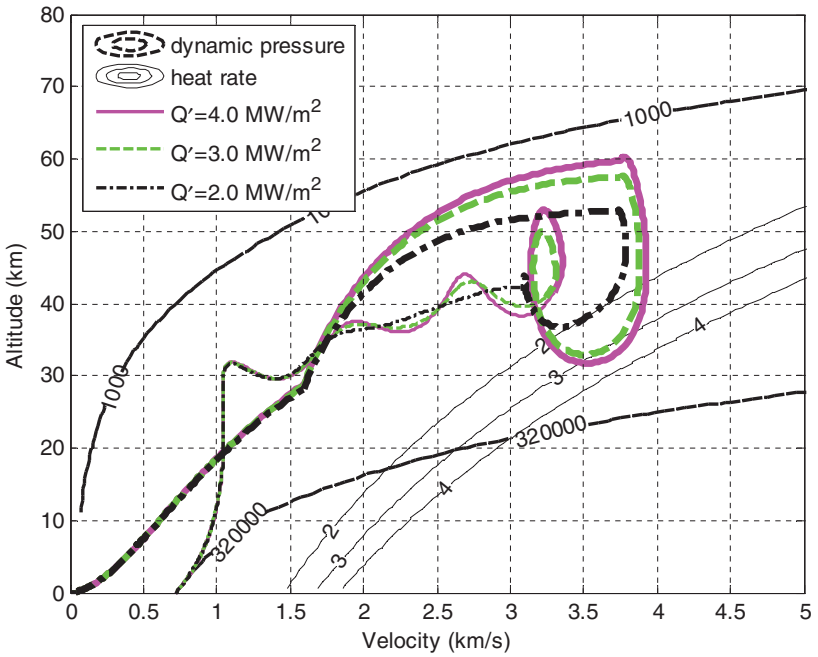

Figure 11. (Colour online) Altitude vs. velocity for surface launch wing-body vehicle with boost phase and objective to maximise the cross-range and different heat rate constraints.

Figs 11-13. Table 3 shows that the cross-range performance reduces by 2.5% once the maximum heat-rate is reduced from 4 MW/m^2 to 2 MW/M^2 value. Figures 11 and 12 show the trajectory shapes on the altitude vs. velocity map with overlaid heat rate boundaries. It can be seen from the figure that for the trajectories with lower heat rate bound, optimal burn-out angle is low, which results in lower burn-out altitude, and therefore, more energy loss due to drag force occurs. Hence, there is very slight loss in cross-range performance. The angle-of-attack, bank angle and throttle control as a function of time are shown in Fig. 13 (a), (b) and (c), respectively. The control deflections, normal acceleration and the path constraints, all remain within limits.

The comparison of results for a rocket assisted wing-body with the wing-body boost-glide vehicle shows that the down-range performance of the rocket assisted wing-body vehicle is 21.7% more than the wing-body boost glide vehicle. Similarly, the cross-range performance is almost 50% more for the rocket assisted wing-body vehicle as compared to the wing-body boost glide vehicle for the medium range launch vehicle under consideration.

The comparison of the rocket assisted wing-body vehicle data with the waverider-type hypersonic boost glide results show that the down-range performance of the rocket assisted wing-body configuration is only 10% lower than the waverider glide vehicle, at one-third integrated heat load computed at the fin leading edge. The reduced heat rate bound data also shows that for 50% reduction in heat rate bound, the performance reduction is less than 9% in the down-range, and 2.5% in cross-range for a rocket assisted wing-body vehicle.

The results suggest that the proposed rocket assisted hypersonic vehicle may be a cheaper and more viable option in the medium to intermediate range hypersonic regime.

https://doi.org/10.1017/aer.2017.11 Published online by Cambridge University Press

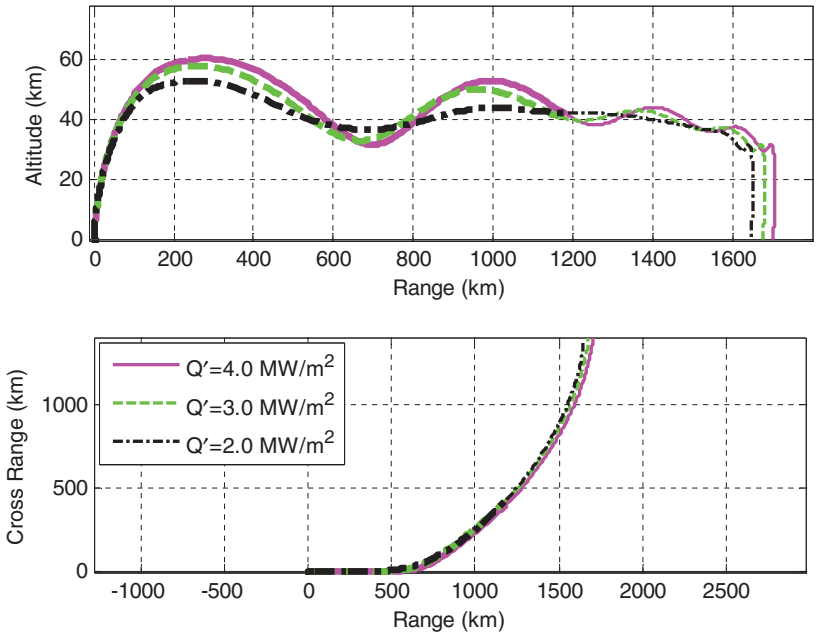

Figure 12. (Colour online) (a) Altitude vs. down-range and (b) cross-range vs. down-range for surface launch wing-body vehicle with boost phase and objective to maximise the cross-range and different heat rate constraints.

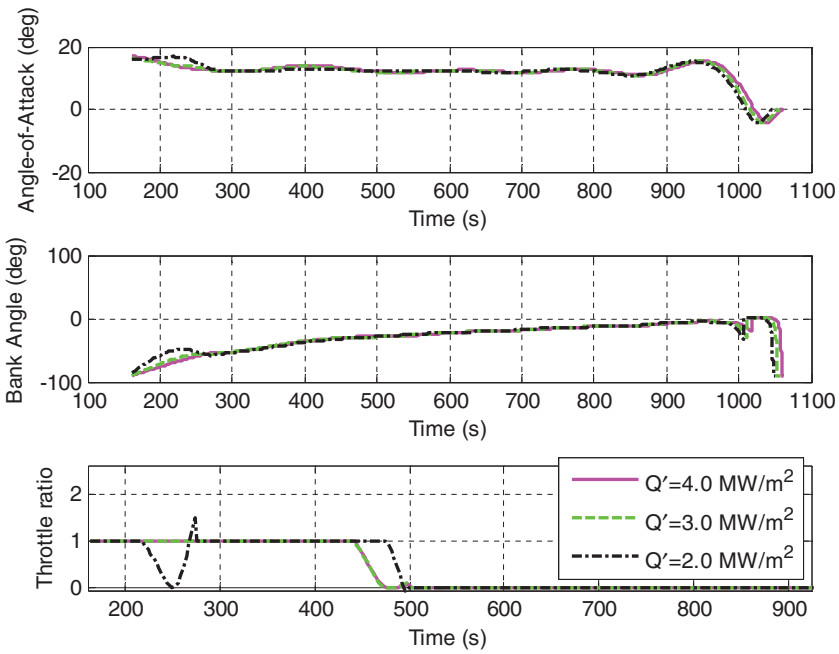

Figure 13. (Colour online) (a) Angle-of-attack vs. time and (b) bank-angle, and (c) throttle-ratio vs. time for surface launch wing-body vehicle and objective to maximise cross-range at different heat rate constraints.

https://doi.org/10.1017/aer.2017.11 Published online by Cambridge University Press

6.0 CONCLUSION

The multiphase, non-linear trajectory optimisation problem has been solved for a rocket assisted wing-body vehicle using the hp-adaptive Pseudospectral method with an aim to compute the best burn-out conditions for the launch vehicle, and the subsequent optimal trajectory, control deflections and thrust time histories, under the constrained heat rate environment, and to maximise the down-range and cross-range performance by modelling the boost phase.

The optimal thrust time histories of the re-entry vehicle show that for the maximum range, the boost phase should start immediately once the burn-out conditions for the launch vehicle are reached. It has been further shown that for a rocket assisted wing-body vehicle and 50% reduced heat rate bound, the performance reduction as compared to the waverider boost glide vehicle, is less than 9% in down-range and 2.5% in cross-range.

The comparative performance analysis between the hypersonic boost glide waverider and the hypersonic rocket assisted wing-body vehicle results show that the down-range performance of the rocket assisted wing-body configuration is only 10% lower than that of the waverider glide vehicle, but at one third integrated heat load computed at the fin leading edge.

These results suggest that a rocket assisted hypersonic vehicle may be a cheaper and a more viable option as compared to a waverider vehicle, in medium to intermediate range hypersonic regime, to achieve the required down-range performance.

REFERENCES

1. CROCKRELL, C.E., HUEBNER, L.D. and FINLEY, D.B. Aerodynamic performance and flow field characteristics of two wave-rider derived hypersonic cruise vehicles, AIAA 33rd Aerospace Science Meeting and Exhibit, 1995, Reno, Nevada, US, AIAA Paper 95–0736.
2. WHITMORE, S.A. and DUNBAR, B.J. Orbital space plane: Past, present, and future, IAA/ ICAS International Air and Space Symposium and Exposition, 2003, Dayton, Ohio, US, AIAA-2718.
3. SURBER, T.E. and OSLEN, D.C. Shuttle orbiter aerodynamic development, *J Spacecraft*, 1978, **15**, pp 40-47.
4. LEY, W., KLAUS, W. and WILLI, H. *Handbook of Space Technology*, vol. 22, 2009, John Wiley & Sons, Munich, GmbH.
5. ZIMMERMANN, F. and CALISE, A.J. Numerical optimization study of aeroassisted orbital transfer, *J Guidance Control and Dynamics*, 1998, **21**, pp 127-133.
6. GOGU, C., MATSUMURA, T., HAFTKA, R.T. and RAO, A.V. Aeroassisted orbital transfer trajectory optimization considering thermal protection system mass, *J Guidance Control and Dynamics*, 2009, **32**, pp 927-938.
7. HULL, D.G. and SPEYER, J.L. Optimal reentry and plane change trajectories, *J Astronautical Sciences*, 1982, **30**, pp 117-130.
8. ZHOU, H., CHEN, W. and YIN, X. Hypersonic vehicle trajectory design based on optimal control theory, Sixth International Symposium on Instrumentation and Control Technology: Sensors, Automatic Measurement, Control, and Computer Simulation, 2006, pp 63582L-63582L.
9. ROSS, I.M. and NICHOLOSON, J.C. Optimality of the heating-rate-constrained aero cruise maneuver, *J Spacecraft and Rockets*, 1998, **35**, pp 361-364.
10. CLARKE, K.A., Performance optimization study of a common aero vehicle using Legendre pseudospectral method, vol. MS, 2003, Department of Aeronautics and Astronautics, Massachusetts Institute of Technology, Cambridge, Massachusetts, US.
11. JORRIS, T.R. Common aero vehicle autonomous reentry trajectory optimization satisfying waypoint and no-fly zone constraints, 2007, School of Engineering and Management, Air Force Institute of Technology, Wright-Patterson AFB, Dayton, Ohio, US.

https://doi.org/10.1017/aer.2017.11 Published online by Cambridge University Press

12. LI, Y., CUI, N. and RANG, S. Trajectory optimization for hypersonic boost glide missile considering aeroheating, *Aircr Engineering and Aerospace Technology*, 2009, **81**, pp 3-13.
13. LI, Y. Optimal attack trajectory for hypersonic boost glide missile in maximum reachable domain, International Conference on Mechatronics and Automation, 2009, Changchun, China.
14. RIZVI, S.T.I., HE, L. and XU, D. Optimal trajectory analysis of hypersonic boost-glide waverider with heat load constraint, *Airc Engineering and Aerospace Technology*, 2015, **87**, pp 67-78.
15. RIZVI, S.T.I., HE, L. and XU, D. Optimal trajectory and heat load analysis of different shape reentry vehicles for medium range application, *DefenceTechnology*, 2015, **11**, pp 450-361.
16. DARBY, C.L. and RAO, A.V. Minimum-fuel low-earth-orbit aeroassisted orbital transfer of small spacecraft, *J Spacecraft and Rockets*, 2011, **48**, pp 618-628.
17. HE, L. *Launch Vehicle Design*, 2004, BUAA Press, Beijing, China.
18. BERTIN, J.J. Hypersonic Aerothermodynamics, Hypersonic Aerothermodynamics, 1994, AIAA Education Series, Washington, DC, US, pp 257-262.
19. SCOTT, C.D., RIED, R.C., MARAIA, R.J., LI, C.P. and DERRY, S.M. *An AOTV Aeroheating and Thermal Protection Study*, volume 96, 1985, Progress in Astronautics and Aeronautics, AIAA, New York, US.
20. TAUBER, M.E. A review of high speed convective heat transfer, computational methods, NASA TP-2914, 1989, Washington, DC, US.
21. RAO, A.V. User's Manual for GPOPS Version 4.0, August 2011, Florida, US.
22. GARG, D., PATTERSON, M.A., HAGER, W.W., RAO, A.V., BENSON, D.A. and HUNTINGTON, G.T.A unified framework for the numerical solution of optimal control problems using pseudospectral methods, *Automatica*, 2010, **46**, pp. 1843-1851.

https://doi.org/10.1017/aer.2017.11 Published online by Cambridge University Press